Reflectivity–Rain Rate Relationships for Radar Hydrology in Brazil

R. V. CALHEIROS

University of Bauru and Institute for Space Research, Brazil

I. ZAWADZKI

Université du Québec à Montréal, Canada H3C 3P8

(Manuscript received 20 April 1985, in final form 2 August 1986)

ABSTRACT

In this work a method is presented to obtain R–Z_e relationships through comparison, in probability, of nonsimultaneous measurements of Z_e and R. Range dependent relationships obtained in this way are given for a radar situated at 20°21'30"S, 49°01'38"W. The method is tested by comparing actual river hydrographs from a number of basins with those simulated using radar data as input to a hydrological model.

1. Introduction

The basic problem of modern hydrology in relation to discharge forecasting reduces to the study of small catchment areas because of the characteristics of the models it relies upon. This requires a knowledge of areal rainfall distribution with an adequate spatial resolution. In tropical regions, where the highly variable convective precipitation predominates, the description of the rainfall field becomes a very serious problem. Such is the situation in a country like Brazil, especially in the very important hydrological area represented by the state of Sao Paulo, on which this work is focused. According to Peck's (1980) discussion of the state of the art of measurement of precipitation, current ground-based measurements are not suitable to properly reproduce the precipitation field. The real-time requirements of operational hydrology adds substantially to the problem. On the other hand, weather radar provides continuous time and space rainfall measurements that is immediately available at a single location and it is able to produce, in real time, detailed information on precipitation over large areas (of the order of thousands of square kilometers) with good spatial resolution (from less than one square kilometer to a few square kilometers). Thus, radar is appealing as an alternative to supply the required rainfall information. With the recent technological advances in digital data handling, weather radar could be implemented operationally for hydrologically oriented area rainfall measurements.

Radar rainfall quantification is affected by many factors; those related to the distance between the radar and the observed precipitation stand out with a consequent loss in precision. Since the range to which radar can be useful will determine the number of radar units required to cover a number of catchment areas, this factor has obvious economical implications, especially for a country like Brazil possessing such large continental dimensions and a vast hydrological network.

The relation of radar observations to rain rates at the ground for hydrological application can be obtained either through a theoretical or an empirical approach. In the theoretical approach, the various factors affecting the precision of the radar measurements must be taken into account, particularly those related to the radar–rainfall distance. Because of the multiplicity of these factors (Zawadzki, 1984), this constitutes a difficult task. An empirical relationship between radar and rain gage measurements derived through correlation techniques bypasses the problems of the theoretical approach with two limitations: first, it permits correct radar estimates of the rain rate on the average only, and second, it requires a long time series of simultaneous measurements by radar and a large number of rain gages located at various distance within the radar range. This last limitation is serious, since such dense rain gage networks are not usually available and they are too costly to implement.

A means of overcoming this difficulty is presented in this paper. It is based on the concept that if two random variables [radar reflectivity factor for rain (Z) and the rainfall rate at the ground (R) in our case] are functionally related, the correct transformation of one into the other will produce equal probability densities $p(Z)dZ$ and $p(R)dR$; i.e., pairs of (R_i; Z_i) that make

$$p(R_i)dR = p(Z_i)dZ$$

define the Z–R relationship.

Alternatively, the desired relationship may be obtained from the correspondence between the lower limits of the integrals of the probability densities

$$\int_Z^\infty p(Z)dZ = \int_R^\infty p(R)dR.$$

This idea was applied to nonsimultaneous radar and rain gage data. Radar data to generate the probabilities $p(Z)$ were obtained from one season of observations from a radar situated in Bauru, near the center of the state of Sao Paulo and covering a climatologically homogeneous area. The gage data used to calculate $p(R)$ curves were extracted from an 8 yr climatologically suitable record of a rain gage with a rainfall distribution typical for the radar coverage area. Since the effects that depend on the range of precipitation were of main concern, radar data were stratified accordingly.

In section 2, the climatology of precipitation of the region is studied using rain gage records. The rain rate distributions at various points of the region are given, as well as the contribution to the total rainfall of the various categories of rain rate. Section 3 describes the radar operation, radar data format and data storage. Statistics of reflectivity factors of a full rain season are presented, stratified by range and time of the day.

In section 4 the correspondence between rain rates and reflectivity factors is obtained through probability comparison, using the results of sections 2 and 3. A verification of the results is made in section 5, through the comparison of historical hydrographs with those simulated using a hydrological model with inputs of radar-derived rainfall fields, with and without range corrections.

2. Rain gage data and rainfall regime in the radar coverage area

To derive the range dependent R–Z_e relationship by the method proposed here, the climatological homogeneity of rainfall regime in the area considered is essential. Consequently, an assessment of this homogeneity was carried out. First, the average yearly rainfall data were considered for 212 rain gages in the state of Sao Paulo, with record length varying from 11 to 33 yr. Those gages are represented by dots in Fig. 1. Using the official classification of hydrological zones in the state, as depicted in Fig. 1, it was verified that zones 1, 2, 3, 4 and 8 show average yearly values around 1259 mm, while zones 6 and 7 present distinctive regimes with values near 1379 mm. Zone 5 is very different with 2095 mm.

It was noted that with the only exception of a minor area in the seventh zone to the northeast, average yearly

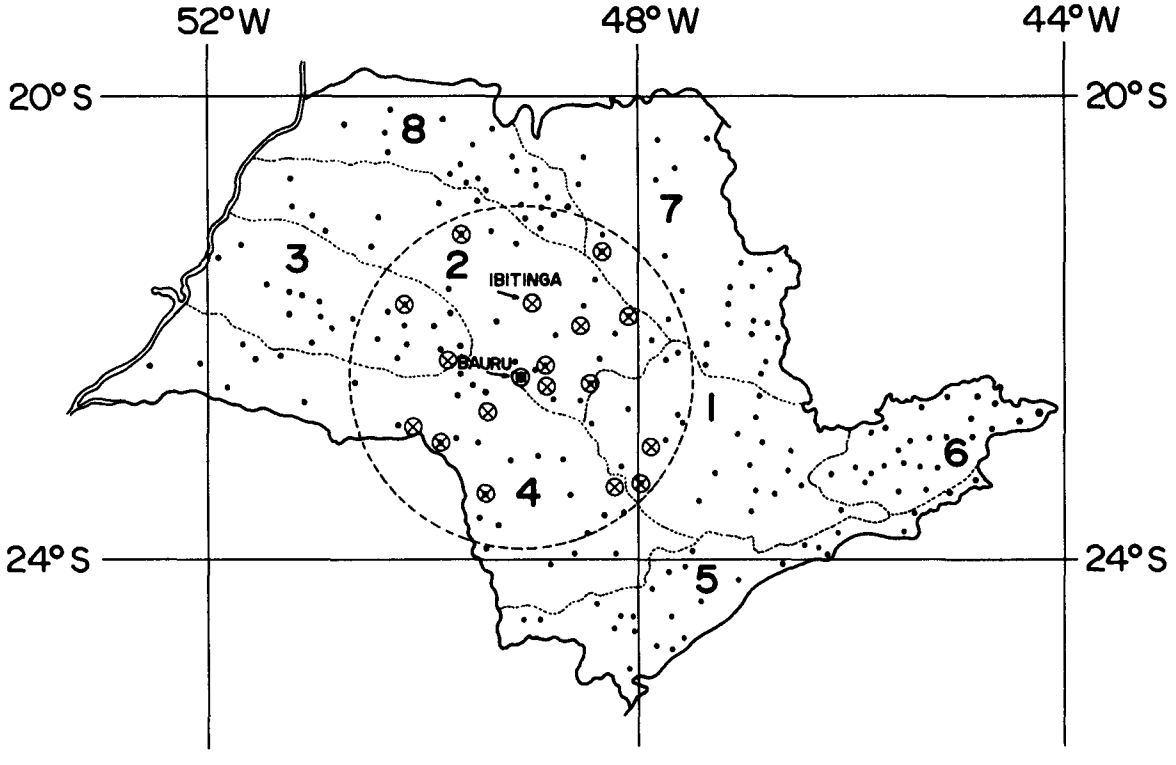

FIG. 1. Hydrological zones of the State of São Paulo, Brazil. Dots indicate pluviometric stations. Dashed circle indicates the radar covered area (radius of 157.5 km). Crossed circles indicate raingage stations used to study the rainfall climatology described in the text.

rainfall values do not differ significantly within the radar coverage area. The relative variability of the yearly rainfall values remains within a narrow interval of 14 to 17%.

Next, a focus on the radar-covered area was made and the isohyetal map on Fig. 2 was analyzed to select one gage representative of the area. The map represents average yearly values from a 30 yr period for the October–March rainy season. From this analysis, as well as data availability and quality, we selected the rain gage at Ibitinga (21°45'S, 49°0'W; altitude: 350 m MSL; Hellmann type gage with a daily chart). This gage is located in a region where average yearly rainfall is between 950 and 1000 mm, while the radar-covered area registers extreme values from under 850 mm to over 1200 mm (see Fig. 2).

Good quality data were available for the period 1971–78, corresponding to eight October–March rainy seasons. To verify further the climatological representativeness of the Ibitinga gage and compare the October 1981–March 1982 rainfall totals (the period of the analyzed radar data) with the average seasonal rainfall totals for the 1971–78 period, 18 gages, identified by crossed circles in Fig. 1 (Ibitinga included), were selected. They are distributed as uniformly as possible over the area of interest. The eight-season mean rainfall total for the 18 gages was 1084.5 mm with a standard deviation of 111.9 mm, while the corresponding Ibitinga gage average was 1062.0 mm; i.e., the Ibitinga gage can be considered as representative of the rainfall climatology of the region. On the other hand, the 1981–82 gage-overgage rainfall was 936.5 mm, indicating a dryer-than-average year.

Thus, the period from which radar data were extracted had rainfall 1.16 times below the climatological value. This factor will be used later to upgrade the sta-

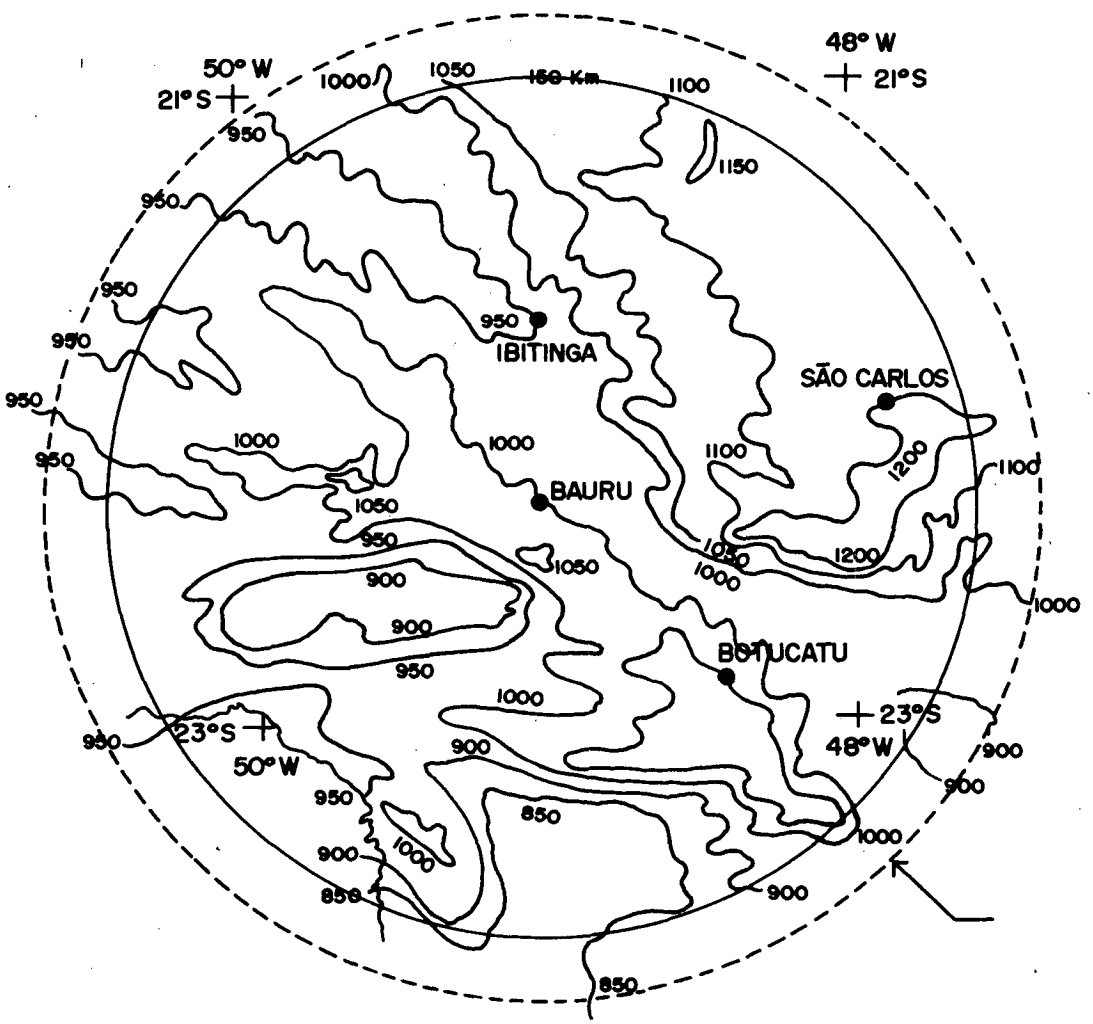

FIG. 2. Average precipitation totals for the rain season from October to March obtained from pluviometric data from the stations in Fig. 1 for data from 1941 to 1970.

tistics of reflectivity in order to render these comparable to the statistics derived from the eight seasons of rain gage data.

Basic pluviometric data were for 10-min average rainfall rates which could reliably be extracted from the records. The following statistics were computed: (i) cumulative probability that a given rainfall rate was equal or exceeded, represented by $P(R' \geq R)$; (ii) fractional contributions (F.C.) to the total precipitation by rain rates smaller than a given value, defined by

$$\text{F.C.} = \int_0^R Rp(R)dR \Big/ \int_0^\infty Rp(R)dR.$$

A stratification of the statistics was performed for the daily intervals 0000–0600 h, 1500–1800 h, 0600–2400 h and 0000–2400 h (local times) to separate the peak activity in the summer afternoon from the less unstable nocturnal regime.

In the case of statistics of the preceding item i, probability curves for the interval 0000–2400 h and for several time resolutions (Δt = 20, 30, 60 and 120 min) of the rain gage records were calculated to verify the stratification of the probability distributions as a function of the smoothing time interval of the records (see Druf-

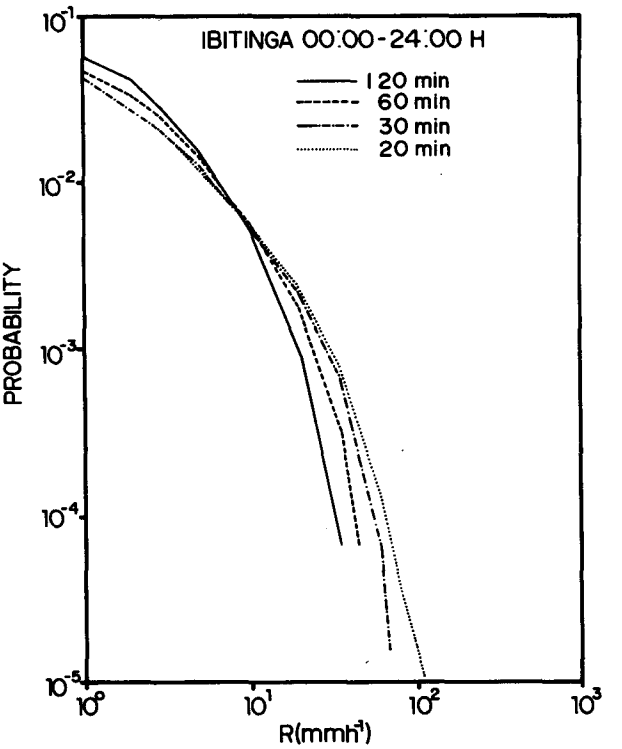

FIG. 4. As in Fig. 3 for the entire 24-h period and for various time resolutions.

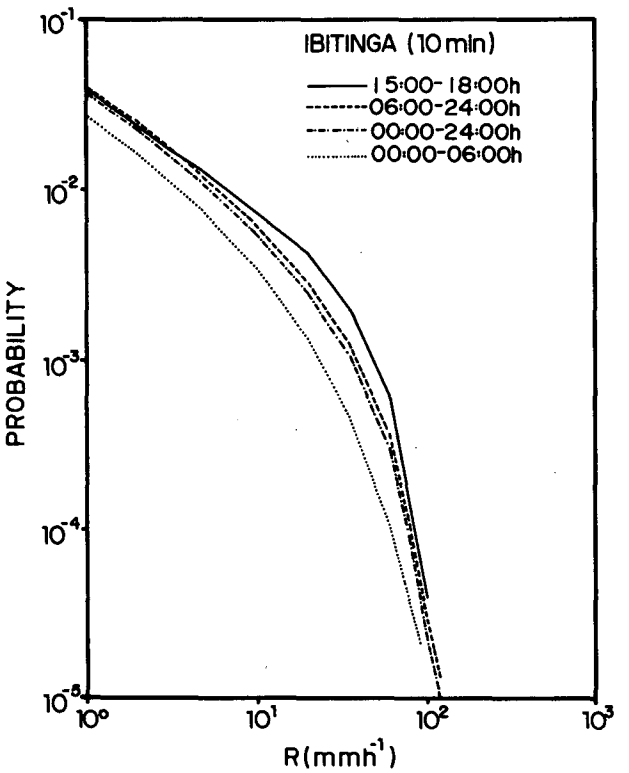

FIG. 3. Probability that a rain rate equals or excedes the indicated value for various periods of the day. Data are 10 min accumulations at the Ibitinga gage.

fuca and Zawadzki, 1975). Figure 3 shows the cumulative probabilities, $P(R' \geq R)$, for the different daily time periods for the gage data with 10 min resolution. In Fig. 4 the cumulative probabilities for the several time resolutions are plotted. Figure 5 gives the F.C. curves for the various periods of the day and a time resolution of 10 min. It can be noted (Fig. 3) that the curves for the 0000–0600 h and 1500–1800 h periods are clearly separated, indicating the difference between the rainfall regimes. However, the 0600–2400 h and the 0000–2400 h curves are much closer to the 1500–1800 h curve than the 0000–0600 h curve; the first two are almost coincident in both the lower and upper rain rate values.

The curves of Fig. 4 show a clear stratification of the probability curves with the time resolution of the gage data. Figure 5 verifies that the nocturnal rainfall regime has a substantial contribution from the lower rain rates, with about 48% of the total precipitation coming from intensities smaller than 10 mm h^{-1} and around 9% from intensities smaller than 1 mm h^{-1}. On the other hand, for the period of highly convective activity, those percentages reduce to 30 and 4%, respectively.

Gage data were tested for statistical representativeness in all cases. Figure 6 shows cumulative probability curves similar to those in Fig. 3 for the 0600–2400 h interval, but obtained by randomly separating the original dataset into two sets of approximate equal sizes.

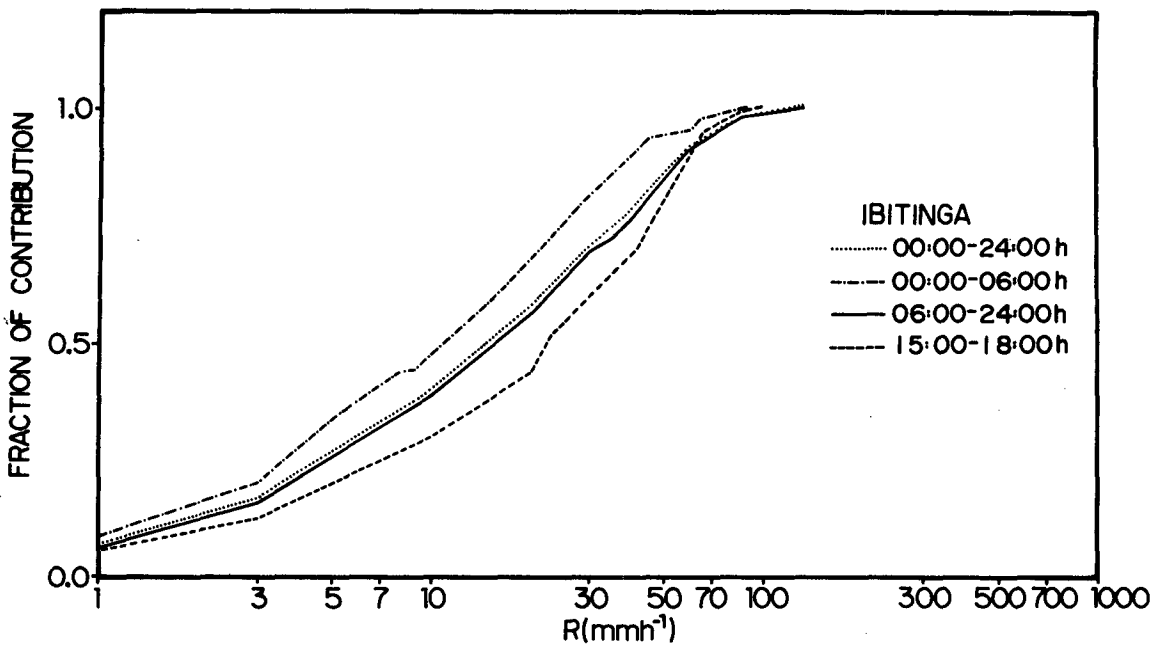

FIG. 5. Fractional contribution to the total rainfall of rates below the indicated value for the indicated periods.

There is no evidence that the sample data were statistically insufficient. This result was also found to hold for all the other statistics from the gage data.

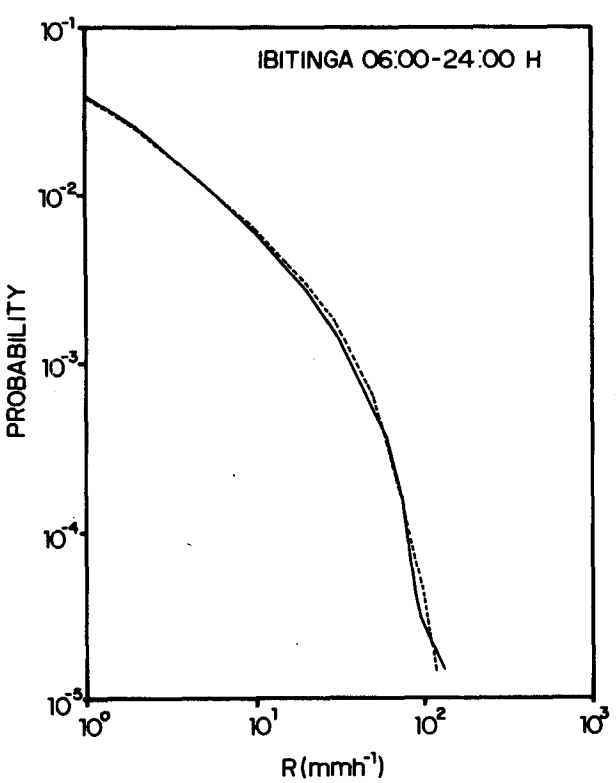

FIG. 6. Cumulative probability distribution of rain rates for two independent datasets (same as for Fig. 3).

3. Radar data

The radar, in operation since 1974, is situated at Bauru in the center of the state of Sao Paulo, Brazil. Radar characteristics are given in Table 1. The antenna scans the space through 15 1-deg steps, from 0 to 14 deg. The duration of the cycle is 5 min. Data, stored on magnetic tape, correspond to 147 range bins (from 3.15 to 157.5 km from the radar) and to every one deg in azimuth. Thus, the radar signal is integrated over 3.5 pulse lengths in range, 14 pulses in azimuth, and it is quantized in 1-dB steps. This integration is quite insufficient to reduce the noise due to the fluctuating radar signal. To eliminate the background noise the software cuts down the signal to -90 dBm (38 dBZ at 100 km). Although this prevents the detection of rates below ~ 10 mm h^{-1} at 100 km, the regime of intense rates present in our region (see Fig. 5) minimized this problem to a certain extent. However, we will see that this is a severe limitation of the system, and our method of transformation of radar measurements into hydro-

TABLE 1. Characteristics of the Bauru radar (ECC WR-100-5).

Characteristic	Value
Peak power	250 Kw
Frequency	5600 MHz
Pulse duration	2 μsec
PRF	259 Hz
2 dB beam width	2° (nominal)
MDS	-106 dBm
Minimum detectable reflectivity factor at 100 km	38 dBZ

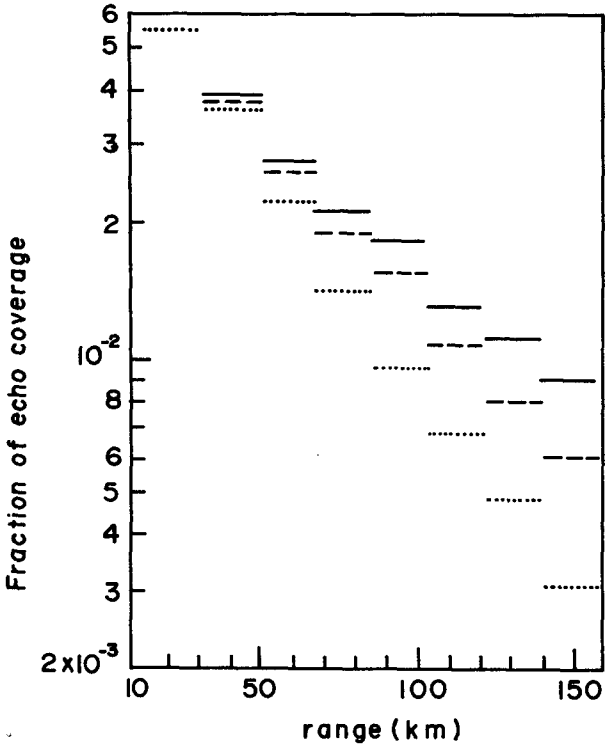

FIG. 7. Solid lines show the average fraction of area covered by radar echo to be expected if the minimum detectable reflectivity (MDZ) was the only range effect present. When attenuation by O_2 is added to the MDZ the dashed lines are obtained. The observed fractional echo coverage is indicated by the dotted lines.

logically useful information takes this problem into account. From these basic records, constant altitude maps (CAPPIs) with a resolution of 4×4 km^2 are readily produced at various heights. The radar is operated continuously and periods of system breakdown are carefully recorded with indications as to the presence or absence of precipitation during the system failure. Daily electronic calibration assures the stability of the radar performance. The values of Z are obtained from received power, using the nominal radar characteristics given in Table 1. The radar data statistics described here were obtained from data collected from October 1981 to March 1982. Data were stratified according to range and time of the day, the latter to account for the different convective conditions apparent in the afternoon (1500–1800 h local time) in a manner analogous to the rain gage data.

Note that the probability of a given radar signal conditional to the occurrence of rain in the radar-covered area is not comparable to the conditional probability of rain gage data, since rain occurs over the radar-covered area much more frequently than over a single gage. Thus, if Z_e is a value of the radar reflectivity factor and Z_o the minimum detectable value of Z_e, we are interested in the *absolute* probability

$$p(Z_e, Z_o) = p(Z_e|Z_o)p(Z_o). \quad (1)$$

Therefore, a careful accounting of the radar operation is essential for the calculation of the probability of rain being detected somewhere on the radar covered area, $p(Z_o)$. In our case, out of the 4380 hours in the season, $N_1 = 3723$ hours were covered by recorded CAPPIs. Some of the N_1 CAPPIs did not contain weather echoes. Those that did contain echoes will be denoted by N_{1p}. On the other hand, $N_2 = 526$ hours were not recorded but it was known from visual observation of the radar scope that during all the N_2 hours, echoes were present in the area. There were $N_3 = 131$ hours when data were not recorded, and it was not known if rain was present in the area.

We assumed that a) the distribution of echo intensity levels during the N_2 hours was as in the N_{1p} hours, and b) echoes were present during the N_3 hours in the same proportion and with the same distribution as during the period for which the CAPPIs were recorded. Thus, N_3 can be ignored for the purpose of our calculations. With these assumptions $p(Z_o)$ was obtained from

$$p(Z_o) = (N_{1p} + N_2)/(N_1 + N_2) \quad (2)$$

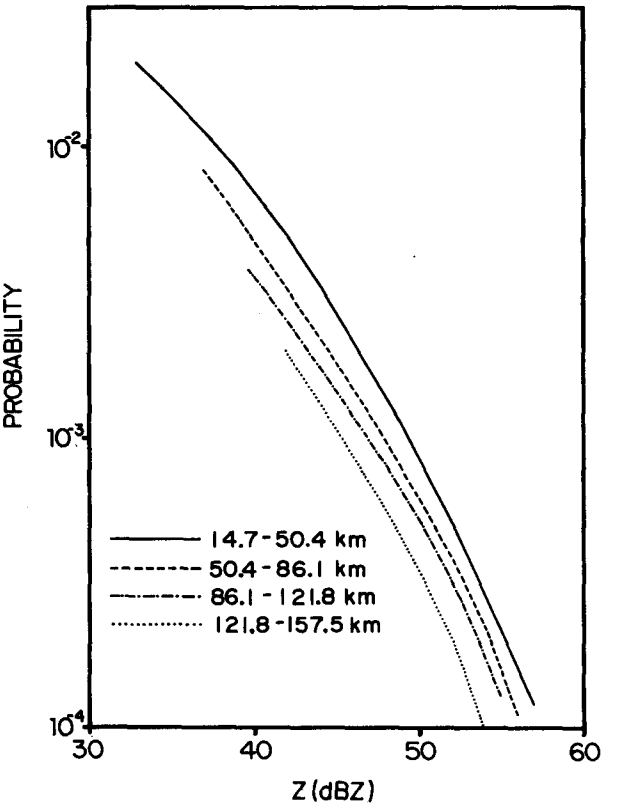

FIG. 8. Probability that the reflectivity factor equals or exceeds the indicated values within the indicated range intervals during the 0600–2400 h period and for the October–March season. Data were extracted from 4 km constant-altitude maps; the space resolution was 1 km $\times 1°$.

where N_{1p} is the number of recorded hourly CAPPIs for which echoes were present somewhere in the region. Statistics of reflectivity factors were obtained from one out of every four CAPPIs in the N_{1p} hours in the form of conditional cumulative probability

$$p(Z' \geq Z_e | Z_o) \approx n_Z/n, \tag{3}$$

where n_Z is the number of bins for which the reflectivity factor exceeded Z_e (dBZ) within the considered area, and n is the total number of bins in that area. Both n_Z and n were counted on the CAPPIs selected from the N_{1p} hours. Thus, the absolute probabilities are

$$P(Z' \geq Z_e, Z_o) = P(Z' \geq Z_e | Z_o) P(Z_o). \tag{4}$$

These statistics were estimated for various range intervals.

Finally, a factor of 1.16 was applied to the absolute probabilities to account for the difference in rain occurrence during this year, as compared to the 8 yr period of the rain gage data. It should be mentioned that since N_2 and N_3 represent only 12 and 3% of the total time, respectively, the uncertainty introduced by our assumptions is negligible.

Let us first consider the fraction of area covered by echoes as a function of distance, i.e.

$$P(Z' \geq Z_{\min} | Z_o) \tag{5}$$

where $Z_{\min}$ is the actual minimum Z_e detected at each range. A number of factors determine $Z_{\min}$: the minimum detectable reflectivity (MDZ) which increases as the square of the range; attenuation by gases (in particular O_2); attenuation by interposed precipitation; increasing height of larger portions of the beam; and beam smoothing in the horizontal dimension. The solid lines in Fig. 7 show the range dependence of the fractional area coverage that one should expect if the MDZ was the only effect present. To obtain this line, the echo area within a progressively higher threshold was determined on the 14–30 km range ring to simulate the inverse-square range effect. In the same way the effect of O_2 was introduced, taking an attenuation of 0.08 dB km^{-1} (Battan, 1973). The dashed line in Fig. 7 shows the combined effect of MDZ and attenuation by O_2. The dotted line shows the actual variation of echo coverage with range obtained from radar data. The difference between the dotted and dashed lines is due to factors other than MDZ and attenuation by O_2. Some of the difference is due to attenuation by water vapor, although it is less important than attenuation by O_2 for the mean humidity conditions in the region. The rest of the difference can be attributed to beam filling, the range increase in the vertical extension of the beam, and also to attenuation by rain, which is not negligible for the C-band radar in the intense rainfall

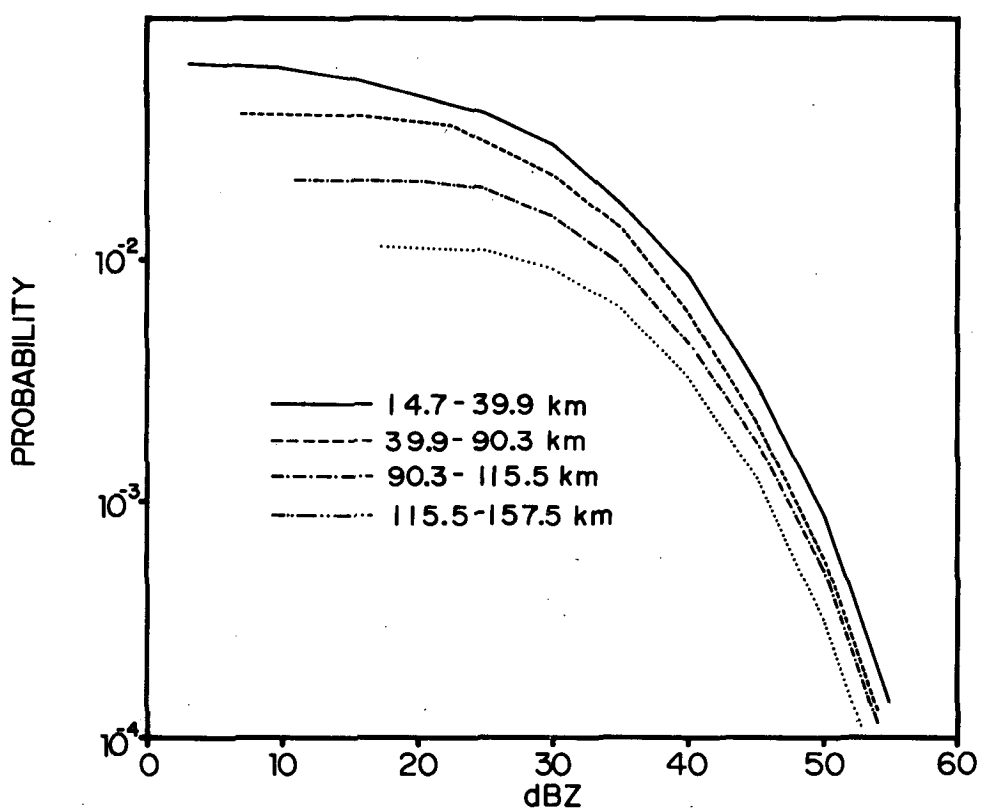

FIG. 9. As in Fig. 8 except that data were smoothed over 4 × 4 km^2.

rate regime of the region. The severity of the problem is apparent, indicating the necessity of some additional range correction if radar data are to be used quantitatively.

The absolute cumulative probability distributions given by (4) are shown in Figs. 8, 9 and 10. All three figures (as well as Fig. 7) correspond to data extracted from 4 km CAPPIs, the lowest CAPPI free of ground clutter and still below the melting layer. The bright band in summer has a mean height of ~5.5 km. Tests with lower CAPPIs have shown that they were affected by excessive ground clutter at short ranges and shadowing at long ranges. Fig. 8 shows the cumulative absolute probability of values of the reflectivity factor in the 1.05 km × 1 degree bins, while Fig. 9 and Fig. 10 were obtained from CAPPIs in which the measurement cell was 4 × 4 km^2. Note that smoothing at the edges of echoes extends the range of dBZ toward lower values. In Figs. 9 and 10 the range intervals used were chosen for best stratification.

It should be pointed out here that no range correction nor direct attenuation correction for O_2 or water vapor was made to the radar data described here. All of these corrections are included in the procedure described in section 4.

4. The transformation of radar data into rain rates

As mentioned in the Introduction, our objective is to establish a correspondence between the measured radar reflectivities and rain rates at ground. For this we will derive a transformation of Z_e into R such that the cumulative probabilities of the two quantities become identical; i.e., we seek the pairs Z_e–R such that

$$\int_{Z_e}^{\infty} p(Z_e|Z_o)p(Z_o)dZ_e = \int_{R}^{\infty} p(R|R_o)p(R_o)dR. \quad (6)$$

A relationship derived from (6) insures that, in the long run, all the moments of the radar-derived rain rate distribution equal the moments of the actual distribution of rain rates at ground. In particular, the long-term average (or accumulation) will be correctly estimated. The advantages of this method, as opposed to correlation techniques, are several: it can be applied to existing data even if rain gage records are not simultaneous with the radar data; it easily lends itself to

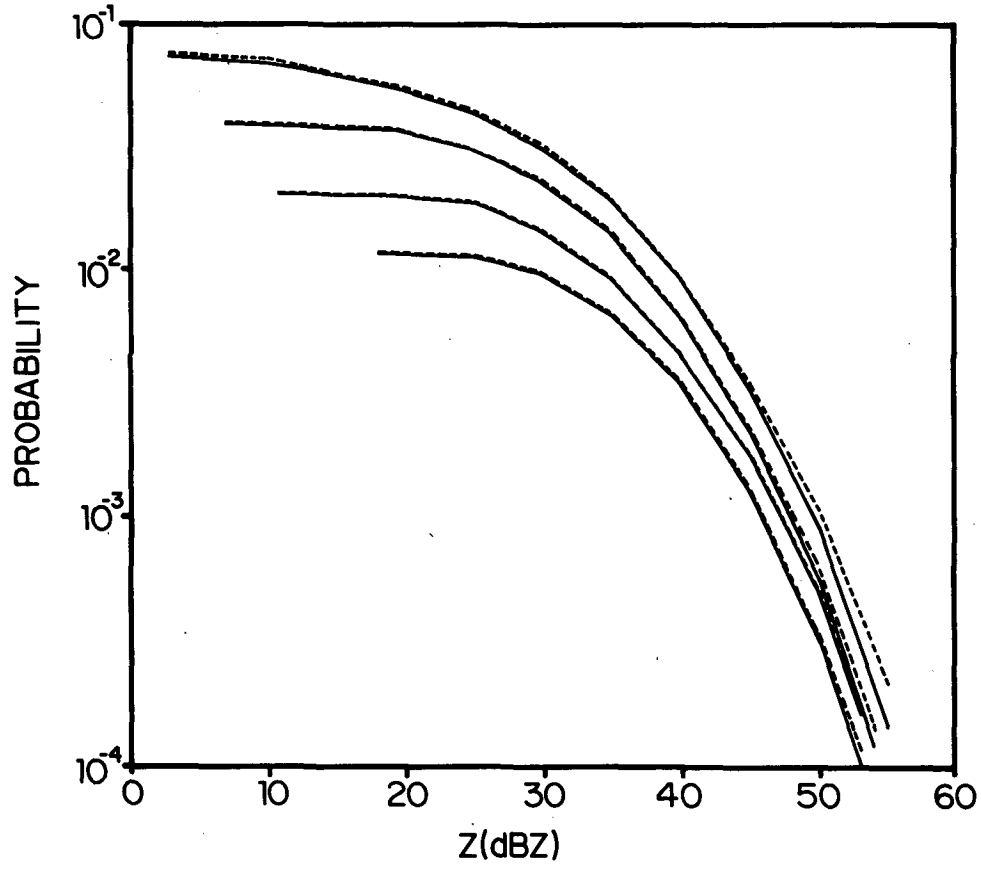

FIG. 10. As in Fig. 9 with data divided in two randomly determined groups (indicated by the solid and dashed curves).

stratification with range without the need of a large number of gages in the region (a long record of one gage is sufficient as long as the climatology of the precipitation is uniform over the region); it readily reveals departures from a power law in the Z_e–R relationship. However, relationships derived by comparison of probability will give good operational results only if each rainfall estimate includes enough values of rain rate to approach a climatological sample. Also, storm to storm variabilities will not be accounted for unless a stratification of the relationship with storm types is performed.

The idea of deriving a relationship through a comparison in probability was applied by Drufuca (1977) to calibrate radar data. Earlier, Miller (1972) derived a climatological Z_e–R relationship comparing probabilities of Z_e and R conditional to the occurrence of rain exceeding a certain intensity; however, the use of conditional probabilities implies that rain exceeding a given value occurs at a point with the same frequency as it occurs over the radar-covered area. This is one of the errors to be avoided in comparing probabilities.

Another detail which should be noted when applying this method is the amount of smoothing present in the data for which statistics are to be compared. As we have seen in sections 1–3, the distribution of 10 min rain rates differs from the distribution of 20 min rates; the same applies to statistics of Z_e with a 4×4 km^2 resolution as compared to a 1.05 km $\times$ 1 degree bin. Therefore, in comparing distributions, the time resolution of rain gage data should be equivalent to the space resolution of radar data. From the statistical properties of rain structure it was determined (Zawadzki, 1975) that this equivalence can be obtained from

$$1.3\sqrt{A} = vt, \tag{7}$$

where A is the resolution area of the radar data, t the time resolution of gage data, and v the translation velocity of precipitation cells. From other studies in the area, v is known to be $\sim$30 km h^{-1} and therefore a 10 min resolution in gage data corresponds closely to a radar measurement cell of 4×4 km^2. If reflectivity values within a smaller measurement cell are to be compared to rain gage data, these should correspond to a shorter smoothing time.

Figure 11 illustrates a graphical method to obtain the Z–R relationship from cumulative probabilities of Z_e and R. The left-hand scale indicates the absolute cumulative probabilities of Z_e and R to be used with the lower (Z_e) and upper (R) scales for the probabilities of Z_e and R. The right-hand scale indicates R and is to be used for the R–Z_e curve, together with the lower scale of Z_e. In the example given in Fig. 11, the statistics of Z_e correspond to values obtained from the 1.05 km $\times$ 1 degree bins, while the probability of R was obtained by extrapolating the curves in Fig. 4 to a smoothing time of 2.25 min.

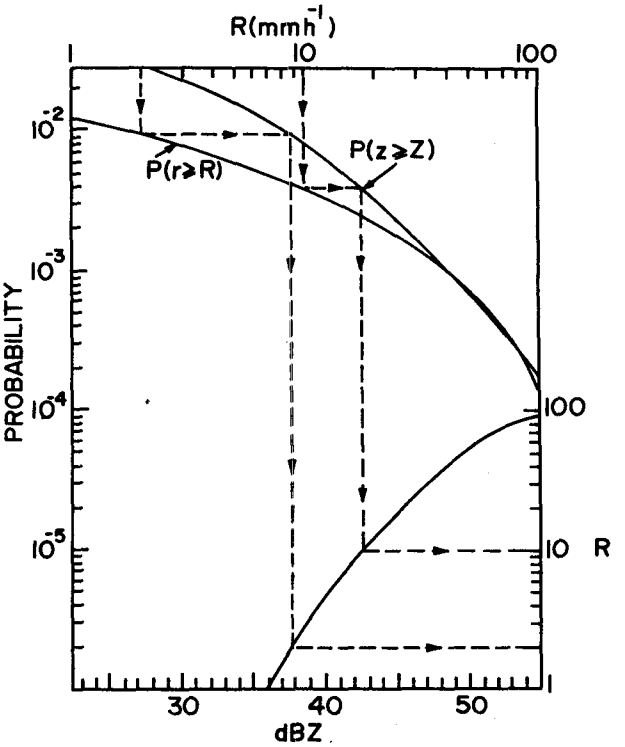

FIG. 11. The lower curve is a R–Z_e relationship obtained graphically from the cumulative probabilities of Z_e and R. The $P(Z' \geq Z_e)$ was obtained from radar data on 4 km CAPPIs in the range interval 15–33 km. Reflectivity data had a resolution of 1 km in range and 2° (beam-width) in azimuth. The $P(R' \geq R)$ was obtained from the Ibitinga gage extrapolated to a time resolutions of 2.25 minutes. The arrows indicate the graphic procedure: from a rain rate of 2 mm h^{-1} (upper scale) the $P(R' \geq 2)$ is determined; the same value of the probability of reflectivity determines Z_e = 37.8 dBZ; thus (37.8, 2) is a point on the R–Z_e curve (plotted on the lower scale of dBZ and the right-hand scale of R).

The range-stratified relationships obtained in this way are shown in Fig. 12 for the 0600–2400 h period and in Fig. 13 for the 1500–1800 h period, for CAPPIs with a resolution of 4×4 km^2. A clear stratification with range and, to a lesser degree, with time of the day is apparent. For reference, two straight lines corresponding to the relationship

$$Z = AR^b \tag{8}$$

have been added to Fig. 12. For short ranges, where radar measurements approximate better the ideal situation, the Z_e–R relationship should approach the Z–R relationship derived from drop-size distributions. Preliminary analysis of 1500 5-min distributions taken in Bauru over a period of 3 months shows that the distrometric values are A = 325 and b = 1.36; i.e., the average slope of the curve for the first range interval in Fig. 12 corresponds well to the distrometric value. However, there is a factor of $\sim$2 between the distrometric and our value of A. The reasons for this discrepancy can be manyfold. Some are physical, such as

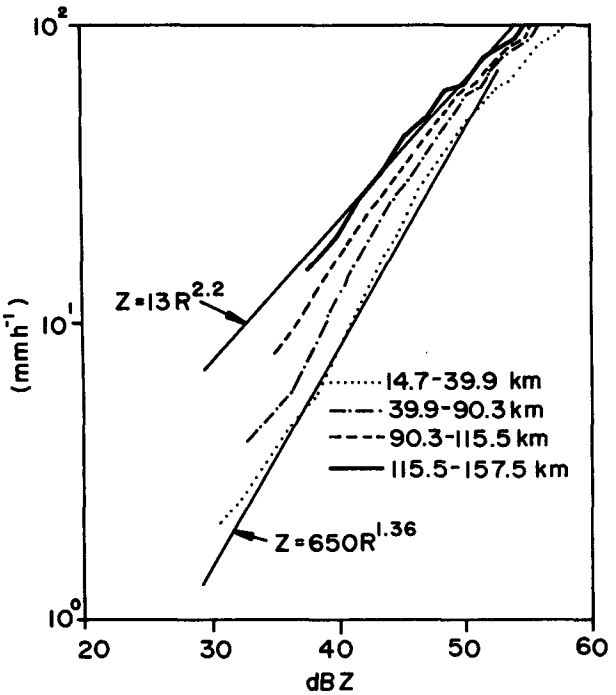

FIG. 12. Relationships of R–Z_e for the period 0600–2400 h obtained by the method illustrated in Fig. 11 for the 4 km CAPPIs. Radar data resolution is 16 km^2; raingage data resolution is 10 min.

evaporation (important for the local dry climate), upward vertical currents at the height of radar measurements, etc.; others could be equipment related. In any case, our comparison of absolute probabilities of Z_e and R provides an absolute calibration for the hydrological application of the radar. Note in Figs. 12 and 13 that, although the average values of A and b change with range, the main range effect can be accounted for by a range-dependent correction factor to be applied to all rain rates. This is particularly apparent for the 1500–1800 (Fig. 13) set of curves which are all fairly parallel to each other.

The transformation of radar measurements into rain rates through the range-dependent R–Z_e relationships derived here ensures that estimates of rain accumulations over relatively large areas and long time periods are unbiased. It does not, however, help to reduce the random errors in the radar-derived rain rates. Neither does it take into account the rain corresponding to Z_e < MDZ. In hydrological practice it could be simpler and equally effective to use a single R–Z_e relationship and apply some range correction factors to rainfall accumulations in a manner reported by Wilson (1976). From the methodology developed here, these correction factors were easily obtained in the following way:

a) Reflectivity data for the 0600–2400 h period from the 4 km CAPPIs were taken, having the BIN as the elementary cell. The data were grouped in eight range rings of 17.85 km in range. For each ring, the distribution of the reflectivity factor Z_e was taken, then Z_e was converted into R through the use of the hydrological R–Z_e relationship derived for the first range ring (shown in Fig. 11), and a value for the precipitation in the jth ring was computed from

$$R_j = \sum_{i}^{Z_{max}} R_i n_{Z_i}, \tag{9}$$

where

j (1, . . . , 8) order number of the ring
i dBZ class, with 1 dB resolution
n_{Z_i} number of occurrences of equivalent reflectivity Z_i
R_i rain rate corresponding to Z_i, through the hydrological relationship for the first ring of Fig. 11.

b) Next, a mean MDZ was taken for each ring and was converted to R through the R–Z_e relationships for different rings. Using Fig. 5, the loss resulting from the nondetection of the lower rain rates was determined for each ring. This loss was added, in each ring j, to the rainfall given by (9). The result is the total rainfall in that ring, R_{t_j}.

A correction coefficient C_j is then defined as

$$C_j = \frac{R_{t_1}}{R_{t_j}}, \qquad j = 1, \cdots, 8. \tag{10}$$

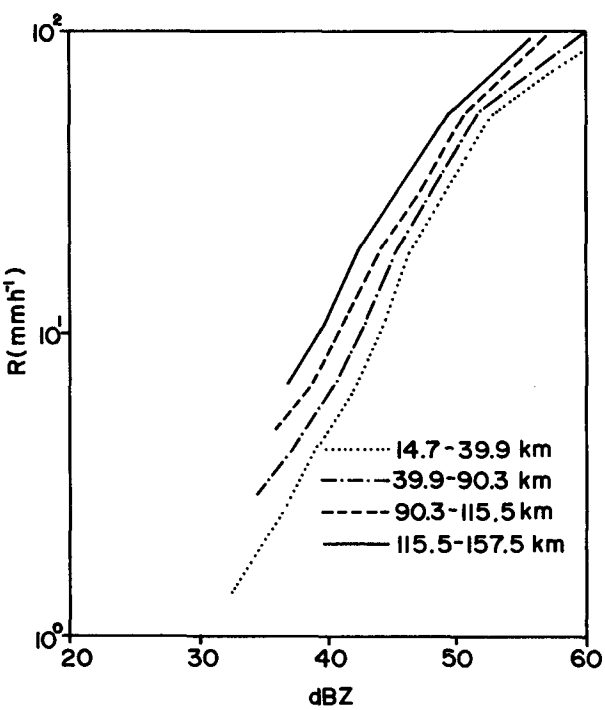

FIG. 13. As in Fig. 12 for the 1500–1800 time period.

The resulting values of C_j are plotted in Fig. 14. Figure 14 can be interpreted as representing the gage-to-radar ratio of cumulative rainfall obtained under the assumption that rain climatology is uniform over the radar-covered area, and all the variation with distance is due to range effects on radar measurements. The correction coefficients C_i are composed of two factors: the variation of R_j/R_1 with range and the undetected contribution to the total rainfall due to the MDZ. The first factor is represented by the dotted lines in Fig. 14 while the combined effect is indicated by the solid lines. For comparison, the dashed curve shows the result obtained by Wilson (1976) for precipitation in conditions where the temperature at 85 KPa exceeded 5°C at Oswego, N.Y. using a direct comparison of hourly rainfall determined by gauges and radar. Given the differences between the Oswego and Bauru radars (particularly the poor sensitivity of the Bauru radar), the nonnegligible attenuation by rain for the Bauru radar and the fact that Wilson's curve was obtained from radar measurements on a low elevation PPI while ours come from a high altitude CAPPIs, the two results compare quite well.

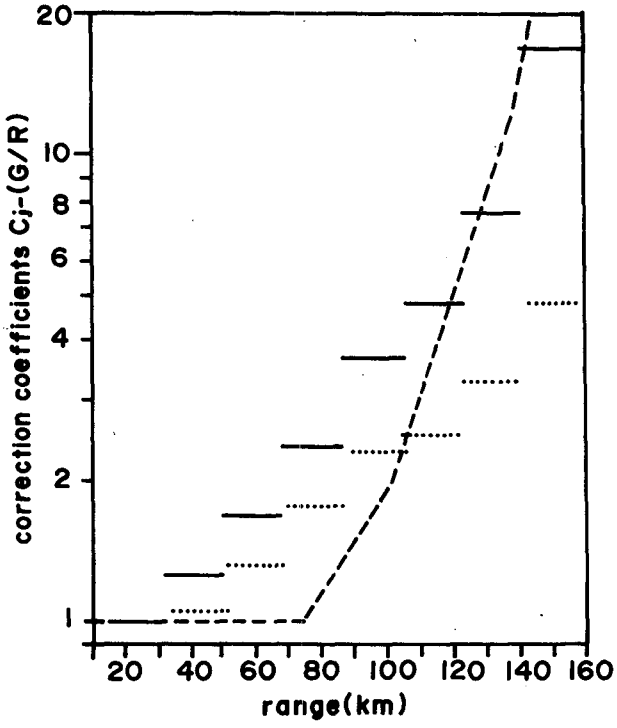

FIG. 14. Range correction factors (gage to radar ratios) for the Bauru radar. Dashed line is from Wilson (1976) obtained by a direct comparison of radar data and rain gage data from a dense network. Dotted lines indicate the correction factors due to the range dependence of the reflectivity to rainrate transformation. In addition, if the contribution of the undetected rain is included in the range correction, the resulting coefficients are indicated by the solid lines.

5. Verification of results

A check was made of the range correction method by a hydrological test using a system called TARTARUS, aiming at the hydrological and hydraulic simulation of a basin and its respective reservoirs and hydropower plants. TARTARUS contains three deterministic algorithms: a) a rainfall-to-discharge conversion model which is the well-known Stanford Watershed Model IV (Crawford and Linsley, 1966); b) a model of wave propagation in channels based on the Muskingum method of routing; c) a model of hydraulic operation. The first part calculates the discharges by unit area generated by the rainfall in each segment of the basin. Model b displaces these discharges by channel reaches, emulating the drainage of the basin. In this way all inflows to the reservoirs are known. The third model performs the necessary iterations to compute the optimal outflow program, as a function of present and future inflow and the desired future water level according to the needs of energy generation, operational constraints, etc.[1] The basic time unit for the inputs (rainfall, potential evapo-transpiration and discharges) is 1 h, while outputs are 24-h averages.

The following procedure was adopted for the test:

a) The basin of the Middle Tiete River as shown in Fig. 15 was selected for the verification. Subcatchments of the basin are distributed along the radar range, making this basin adequate for the test. The outer border of the coverage area in the region of the basin was near fluviometric gage stations, allowing the verification to be independent of the upriver catchment.

b) The 45 day period, from 9 December 1981 to 24 January 1982, within the October–March wet season and coincident with the start of the epoch of highest rainfall, was chosen for the test. The hydrological model is routinely recalibrated at the beginning of October.

For the test, the following points of control were selected:

Barra Bonita Dam (BAB)

Ibitinga Dam (IBI)

Bariri Dam (ASL).

These points are located along the boundaries of the three catchment areas defined in Fig. 15.

Geographically, these areas are distributed at far, middle and near distances, respectively, from the Bauru radar, with the mean distance as follows: Bariri 44 km, Ibitinga 85 km and Barra Bonita 125 km.

In previous years, radar data were used by the hydrologists at CESP in conjunction with rain gage data, or alone when gage data were not available, to predict hydrographs for these subbasins. From this practice

[1] This system is used by the Energetics Company of the state of Sao Paulo (CESP) in the management of its network of dams.

the hydrologists developed empirical adjustments for each subbasin, to compensate for the large discrepancies between predicted and actual hydrographs arising from the uncorrected radar data.

For the test of our results, two sets of data were given to CESP: in the first, reflectivities at all ranges were transformed into hourly rainfall using a single R–Z_e curve (the one derived for the first range ring); the second set of rainfall data were range corrected according to our C_j factors of Fig. 14.

The TARTARUS model was run with the first set as input for all subbasins, with a single calibration coefficient of the hydrological model. This coefficient was the one usually applied to BAB drainage basin and it was selected, first, because this control point is considered by CESP to be the most important of the three and, second, because the model has low response sensitivity to the not very significant rain events present in the other two subbasins. The resulting hydrographs are shown in Figs. 16, 17 and 18 (dash–dot curves). As expected, the BAB hydrograph is fairly well reproduced by the model while the flow of the other two stations

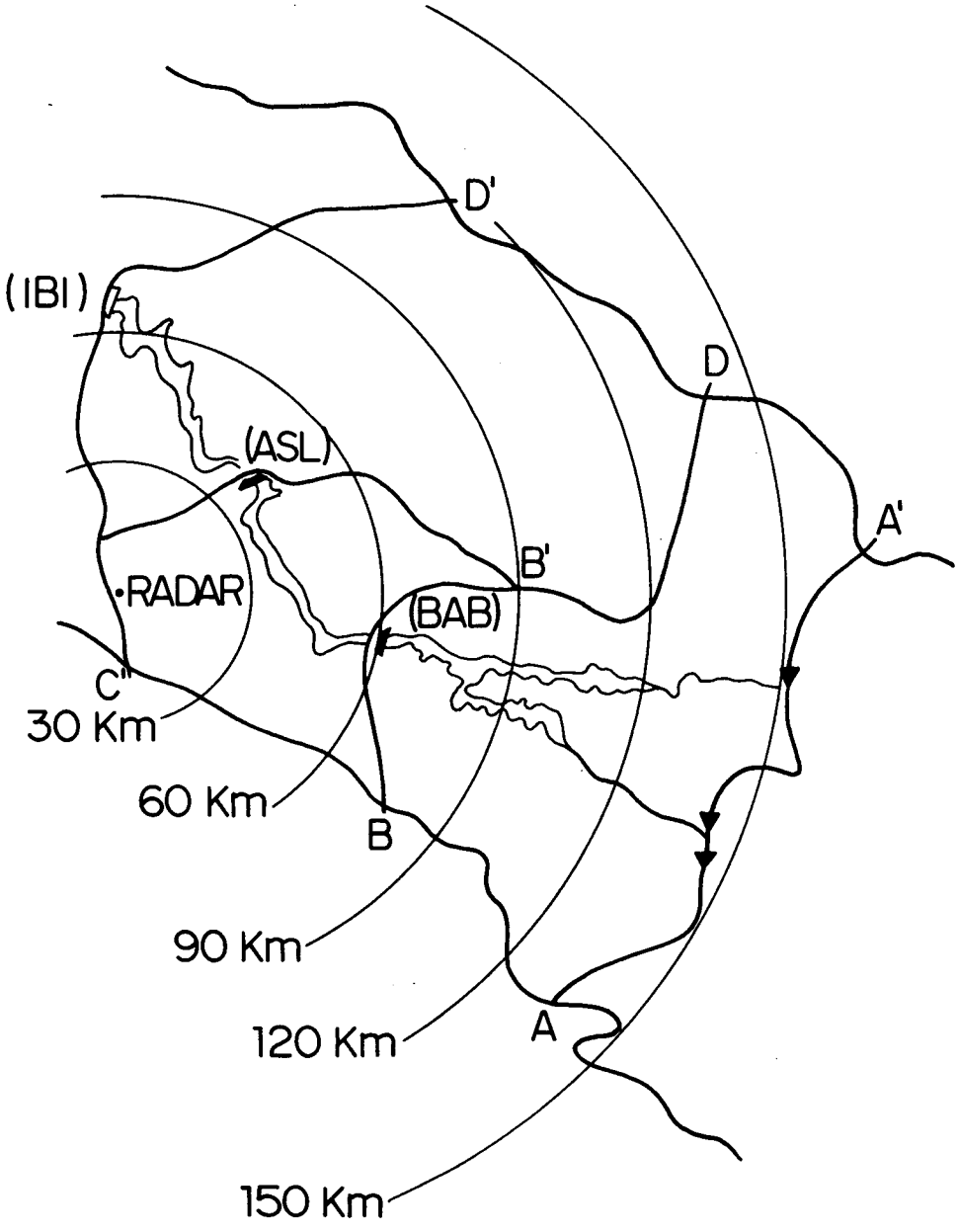

FIG. 15. Drainage basins contributing to the discharge at the dams of Ibitinga (IBI), Bariri (ASL) and Barra Bonita (BAB).

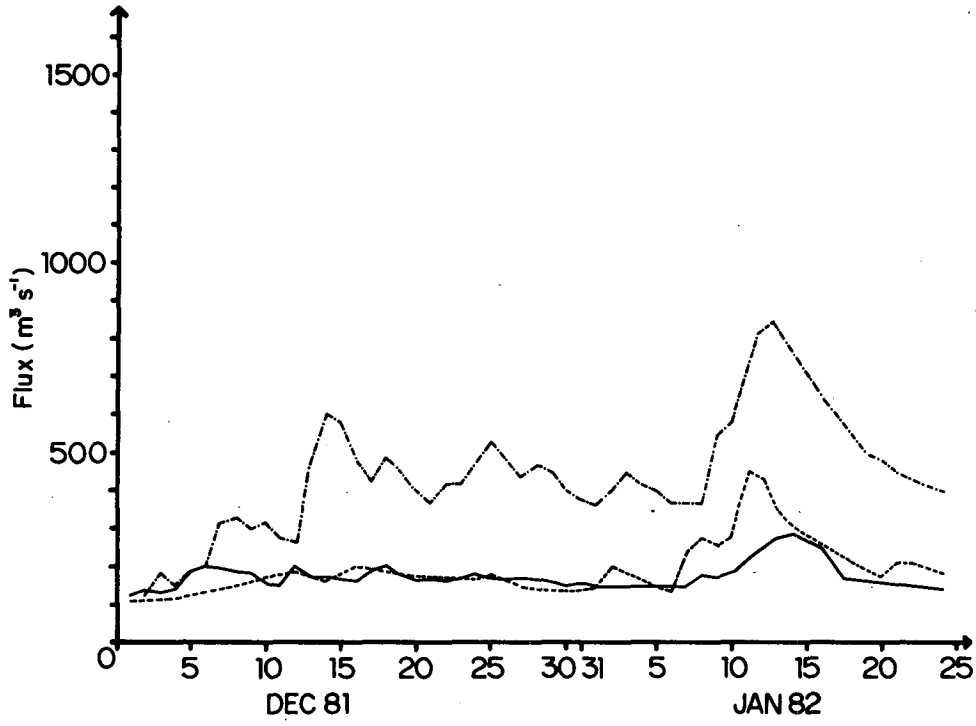

FIG. 16. Hydrographs at Ibitinga: the dashed line shows the actual hydrograph determined at the IBI dam; dash-dot shows the simulated hydrograph using radar data with no range correction; solid line is the simulated hydrograph using range-corrected radar data.

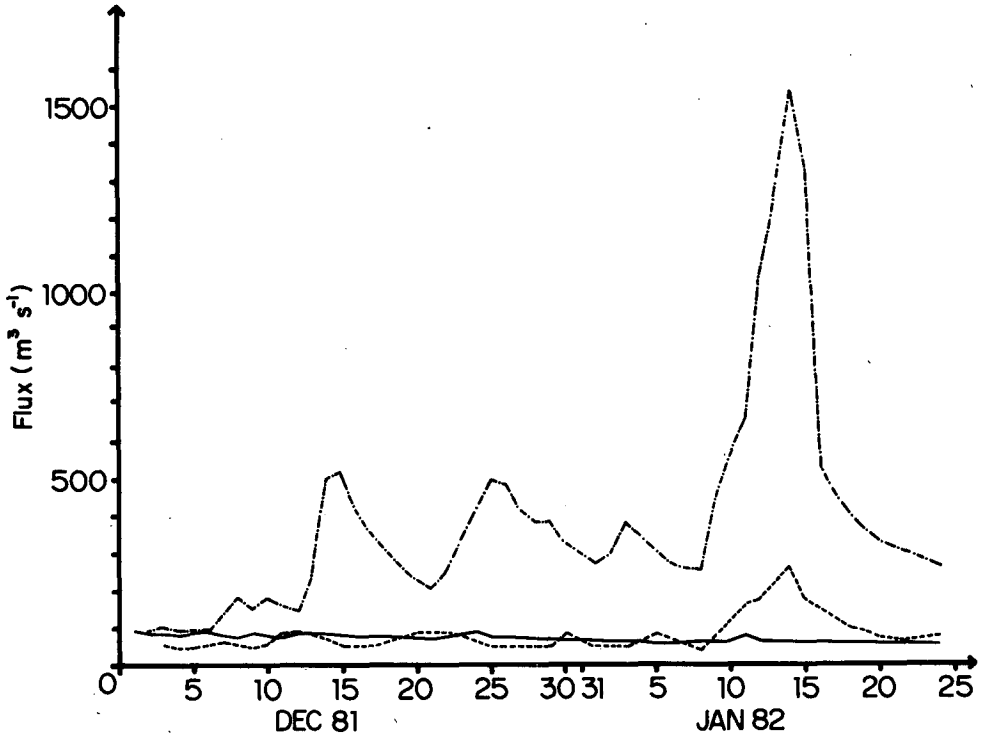

FIG. 17. As in Fig. 16 for the ASL station.

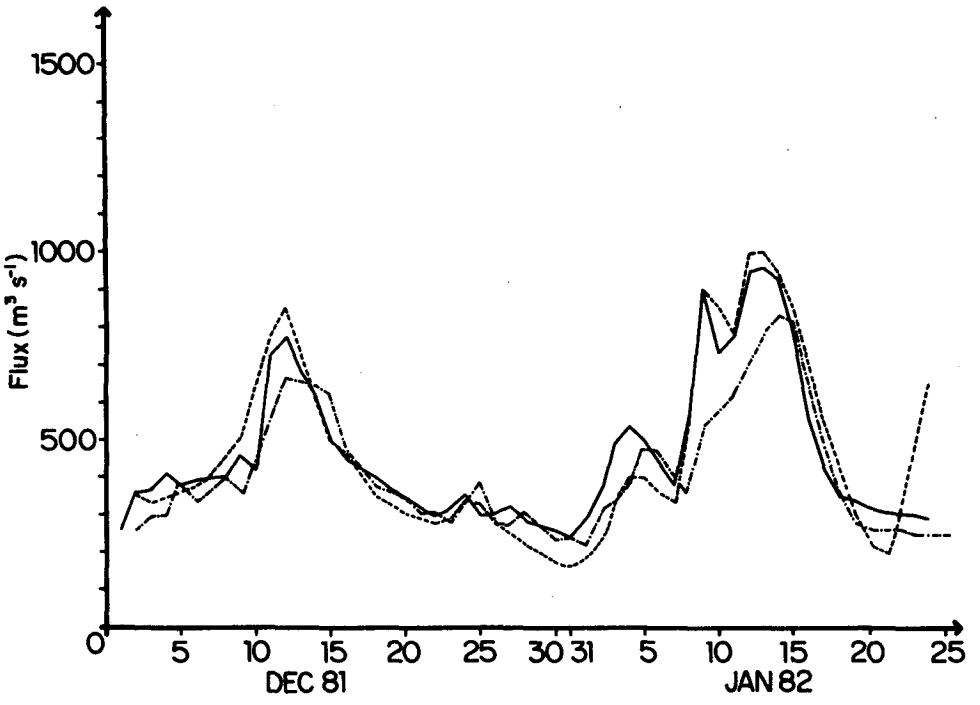

FIG. 18. As in Fig. 16 for the BAB station.

(closer to the radar) is grossly over-estimated (as a result of using the coefficient of the furthermost subbasin).

To introduce the range-corrected set of radar data, all previous adjustment coefficients were removed from the model. Next, the model was calibrated, optimizing again the hydrograph at the BAB station (this calibration is equivalent to applying a single factor to all data). The results are indicated by the solid line in Figs. 16, 17 and 18.

Comparison of the two sets of simulated hydrographs with the actual hydrograph indicates that, first, the systematic discrepancies in IBI and ASL disappear when our range correction coefficients are introduced and, second, the BAB simulated hydrograph (optimized in both runs) is appreciably better reproduced with our range correction. This is because a single coefficient was used in the first run for the entire subbasin while in the second run, the correction coefficient changes with range within each subbasin.

Aside from efficiently removing the gross overestimations at the IBI and ASL stations, our range correction of radar data does not appear to lead to good reproduction of the peaks in the hydrographs. However, as we mentioned before, the model is not calibrated to reproduce correctly the details of low rainfall events. In terms of the water volume estimation, corrected values undoubtedly provided more significant results, having been considered suitable by the users.

A more direct test of the method, i.e., a comparison of radar and rain gage-derived rainfalls, was not possible due to the unavailability of a gage network dense enough for the correct estimation of areal totals. The verification presented is oriented toward the users in the hydrological community. Consequently, the variable verified was the mean daily discharge in control points of the hydrological basin. The reason for using mean daily discharges is twofold: first, there were no control points in the drainage areas allowing the verification of the real hourly discharges; and second, there is no practical need for the values of hourly discharges for the hydraulic operation of the CESP dams. In addition, the TARTARUS model is not calibrated to reproduce the wave shape with hourly resolution.

The factors contributing to the historical discharge values correspond to the inflow to the Barra Bonita dam, the contribution of the drainage area between BAB and ASL (outflow of BAB excluded), and the contribution of the drainage area between ASL and IBI (outflow of ASL excluded). To obtain the historical hydrographs, data from the hydrological budget of the dams were utilized, which permit, after the appropriate analysis, the establishment of the mean discharges.

6. Discussion

In this work we describe in some detail a method to transform radar data into hydrologically useful information. This method, based on the comparison of absolute probability of radar and gage measurements, does not optimize the measurement of individual rain

rates but rather aims at providing estimates of rainfall accumulations. It should give good results provided that it is applied to rainfall over areas and time periods that include a large sample of rates.

The method was tested through a hydrological model and the results seem to confirm the logic behind the transformation of reflectivity to rainfall through comparison of absolute probability. However, the model outputs reflect both the uncertainties in radar measurements of rain and the particular problems related to hydrological simulation. On the other hand this test is user-oriented, and the corrected radar data perform well in those tasks for which the hydrological model was designed: i) a good estimation of volumes in low rainfall events, ii) a good estimation of peak flow, iii) the timing of the peaks, and iv) the volumes in heavy rainfall.

Our statistical approach to relate reflectivity measurements aloft to rain rates at the ground appears to be an inexpensive (in time and resources) technique in response to some of the problems related to radar hydrology. In particular, the stratification of R–Z_e relationships with range and diurnal variability can be obtained from existing records in a simple manner. Although this method will not reduce the large dispersion observed in scattergrams of rain gage-measured rates and simultaneous radar reflectivities, it helps to eliminate a number of systematic errors and brings out the nonlinearities in the $\log Z_e$–$\log R$ plots. Also, it is suitable for further stratification (with storm types, for example). Work is underway to complement our study with pluviographic and distrometric information.

Rain rate-reflectivity relationships for different daily time periods indicate that at least in the tropical areas, specific relations should be used for the convective afternoon period, in particular, in catchment areas of fast response as in urban basins. This might apply also when hourly discharges are simulated by models with relatively small elementary subbasins.

On the other hand, individual R–Z_e relationships should be considered along with the diurnal stratification if local effects are present, as in the metropolitan area of the city of Sao Paulo, where orography interacting with a sea breeze and "heat island" situation determines a very localized rainfall regime.

Acknowledgments. Much of this work was based on the first author's Doctorate thesis (Calheiros, 1982). The author is thankful to both Professor Fazal Hussein Chaudhry, advisor, and the second author who acted as a foreign coadvisor.

Thanks are also due to the CESP—Energetics Company of the State of Sao Paulo—for providing the test with the Tartarus Hydrological Forecasting Model and the helpful comments from their hydrologists. Dr. P. Zwack's editing of the manuscript is appreciated.

REFERENCES

Battan, L. J., 1973: Radar Observations of the Atmosphere. University of Chicago. pp. 324.

Calheiros, R. V., 1982: Resoluçao Espacial de Estimativas de Precipitaçao com Radar Hidrometeorologico. Dr. Thesis, Sao Carlos Engineering School, University of Sao Paulo EESC/USP, 230 p, available from the library of the Escola de Engennaria de Sao Carlos/USP, Ave. Carlos Botelho, 1465, 13.560 Sao Carlos, SP, Brazil.

Crawford, N. H., and R. K. Linsley, 1966: Digital Simulation in Hydrology: Stanford Watershed Model IV. Stanford University, Dept. of Civil Engineering, Technical Report 39. 57 pp.

Drufuca, G., 1977: Radar derived statistics on the structure of precipitation patterns. *J. Appl. Meteor.* **14,** 1419–1429.

——, and I. Zawadzki, 1975: Statistics of raingage data. *J. Appl. Meteor.* **14,** 1419–1429.

Miller, J. R., 1972: A climatological Z–R relationship for convective storms in the northern Great Plains. *Proceedings, 15th Radar Meteor. Conference,* AMS, Boston, Mass., 153–154.

Peck, E. L., 1980: Design of precipitation networks. *Bull. Amer. Meteor. Soc.*, **61,** 894–902.

Wilson, J. W., 1976: Radar-raingage precipitation measurements: A summary. *Proceedings, First Conf. on Hydrometeorology,* Amer. Meteor. Soc., Boston, Mass., 72–75.

Zawadzki, I., 1984: Factors affecting the precision of radar measurements of rain. *Proceedings, 22nd Conf. on Radar Meteorology,* Amer. Meteor. Soc., Boston, Mass., 251–256.